JOURNAL OF PROPULSION AND POWER
Vol. 27, No. 4, July–August 2011

Side Loads in Subscale Dual Bell Nozzles

Chloé Génin* and Ralf H. Stark†
DLR, German Aerospace Center, D-74239 Hardthausen, Germany

DOI: 10.2514/1.B34170

The contour inflection of the dual bell nozzle forces the flow to a symmetrical and controlled separation in sea level mode. At a certain altitude, the transition to high-altitude mode takes place: the flow attaches rapidly to the nozzle extension wall, down to the exit plane. During this transition the separation point moves in the extension, generating potential high side load peaks due to its asymmetrical position. A cold flow subscale test campaign has been conducted on three nozzle models at the German Aerospace Center to evaluate the generation of side loads in dual bell nozzles. The phenomenology is given for the different nozzle flow regimes. Both operating modes are related to very low side loads. Transition and retransition induce a strong short time peak. The phase of sneak transition, corresponding to a flow separation within the inflection region before the start of the actual transition, generates comparable side loads to separated conventional nozzles. The influence of the various geometrical parameters on flow behavior and side load generation was also investigated in this study. The extension length is shown to be the critical parameter for flow stability, transition duration, and side load generation, leading to the necessity of a tradeoff for the optimization of the dual bell concept in rocket applications.

Nomenclature

α	=	contour inflection angle, °
ϵ	=	area ratio
I_{sp}	=	specific impulse, s
L'	=	relative extension length, $L' = L_e/L_{tot}$
M	=	Mach number
P_0	=	total pressure, MPa
P_a	=	ambient pressure, MPa
P_w	=	wall pressure, MPa
R_{th}	=	nozzle throat radius, mm

Subscripts

1, 2, 3	=	refers to the nozzle contours DB1, DB2, and DB3, respectively
b	=	base nozzle
e	=	extension nozzle
init	=	initial length of the nozzle model, before truncation
tot	=	total
tr	=	transition from sea level to high-altitude mode
retr	=	retransition from high-altitude to sea level mode

I. Introduction

TODAY'S European heavy lifter Ariane 5 features a parallel staged design, where a cryogenic main stage is supported by two solid boosters generating the main part of the liftoff thrust. Its original objective was to deliver heavy payloads to a low Earth orbit. Nowadays Ariane 5's dual GTO payload capability is in focus. In opposition to tandem-staged rocket systems, like Ariane 4, the main stage engine Vulcain 2 has to be ignited on the ground for security reasons to assure proper running before solid boosters' ignition and rocket takeoff. Because of this design concept, the main stage engine has to fulfill a wide range of operation conditions, from sea level to near vacuum. To reduce undesired side loads that would affect the engine, the rocket structure, and even the payload itself, the nozzle area ratio is limited, preventing flow separation at sea level. This area ratio limitation leads to performance losses as the engine's exhaust flow is driven overexpanded at sea level and highly under expanded at high altitudes. To optimize the overall I_{sp} of an engine during ascent, the use of altitude-adaptive nozzles, where the thrust generation is not only optimized at one specific altitude, comes into focus as the subsystem with the most promising performance gain. Different concepts were developed to circumvent the limitation in area ratio of conventional nozzles. The commonly discussed solutions are plug, extendible, and dual bell nozzles. The characteristic contour inflection of the dual bell nozzle divides the nozzle into base and extension (Fig. 1) and offers a one-step altitude adaptation.

At sea level, the contour inflection forces the flow to separate controlled and symmetrically (Fig. 2). The base nozzle flows full and the extension is separated: the dual bell is operating in sea level mode. Because of a smaller effective area ratio the sea level I_{sp} increases compared with a conventional nozzle (Fig. 3). At the designed altitude the flow attaches abruptly to the wall of the extension down to the exit plane (Fig. 4). This transition to high-altitude mode results in a short time I_{sp} loss but later on in a higher vacuum performance. The dual bell's major advantage is the absence of any moving parts. Only minor changes to the design and the structure of already operating rocket engines would be necessary.

The concept of applying a contour inflection was first mentioned by Foster and Cowles [1] within a study on flow separation in supersonic nozzles. Various solutions were suggested to prevent uncontrolled flow separation. The one with an inflection dividing the nozzle in two parts was later patented as the dual bell nozzle by Rocketdyne in 1968. The first experimental study was performed by Horn and Fisher [2] with different extension contour design approaches in cold flow subscale tests.

The transition from one operating mode to the other is particularly of interest as the flow potentially separates asymmetrically within the extension, resulting in a strong side load peak.

The dual bell topic was introduced in the late 90s into Europe's community [3]. Hagemann et al. [4] presented in 2000 experimental cold as well as hot flow studies with respect to side load generation. One remarkable fact is that the side load peak during retransition (while the nozzle is shut down) was shown to be significantly higher than during transition. An opposite result is given in studies performed since (e.g., by Hieu et al. [5]) where the transition to high-altitude mode generates higher side loads.

The experimental cold flow results [4] were recalculated at DLR, German Aerospace Center by Karl and Hannemann [6] using the inhouse code TAU. The transient simulations showed that the calculated side load peak during transition mainly depended on the nozzle

Presented as Paper 2010-6729 at the 46th AIAA Joint Propulsion Conference, Nashville, TN, 25–28 2010; received 3 November 2010; revision received 3 February 2011; accepted for publication 8 February 2011.

*Research Scientist, Institute of Space Propulsion, Langer Ground.
†Head of Nozzle Group, Institute of Space Propulsion, Langer Ground.

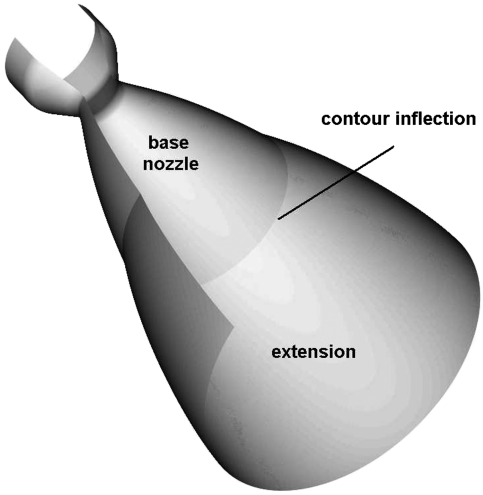

Fig. 1 Dual bell nozzle principle sketch.

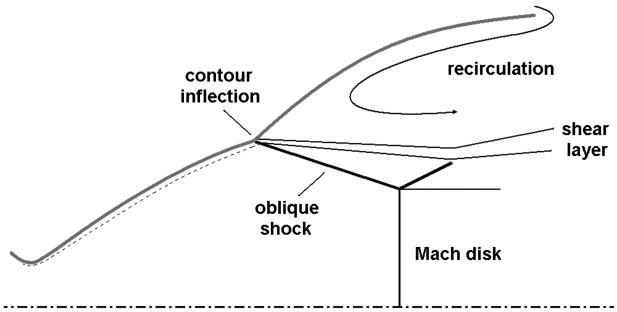

Fig. 2 Sea level mode.

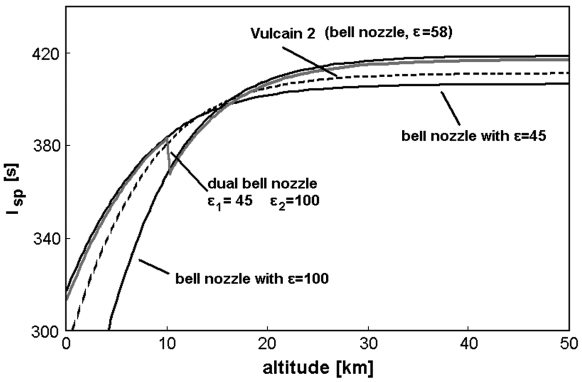

Fig. 3 Impulse generation for conventional and dual bell nozzles.

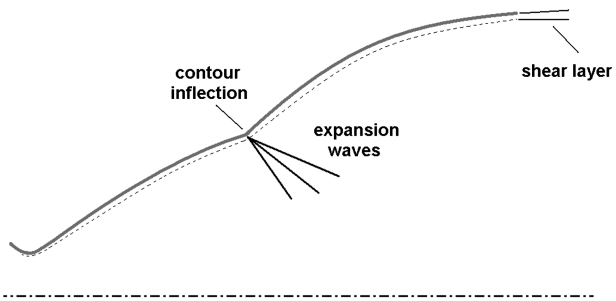

Fig. 4 High altitude mode.

pressure ratio gradient (unfortunately unrealistically high, with up to 2 MPa/ms).

The side load generation was studied in a numerical parametric study by Martelli et al. [7] (2007) as a function of the wall pressure gradient, the base length, the Reynolds number, and the contour inflection angle. The effect of a cooling film applied on full scale hot flow dual bell nozzles is presented in [8]. The dual bell nozzle principle was found to improve the film cooling efficiency compared with conventional nozzles. The side loads generated during the transition increase with increasing film mass flow.

The influence parameters on peak amplitude and duration are up to now not fully understood and should be studied in detail, as side loads are one of the decisive factors for future dual bell nozzle applications.

A cold flow test campaign has been conducted on three different dual bell nozzle geometries at DLR, German Aerospace Center in Lampoldshausen. Wall pressure and side load measurements were made while varying the nozzle pressure ratio (NPR $= P_0/P_a$) with various ramps. The parametric study aimed to identify the influence of the geometry for dual bell contour optimization in future applications.

The present paper introduces the phenomenology of side load generation in dual bell nozzles and gives a detailed experimental parametric study, presenting the influence of geometrical design factors on transition and related side loads.

II. Experimental Setup

A. Test Facility

The tests were conducted at the cold flow test facility *P*6.2 at the Lampoldshausen site. The facility is used to study supersonic nozzles, diffusers, and ejector setups. Two test positions are available: a vertically positioned high-altitude chamber featuring variable chamber pressures and a horizontal test rig for testing under sea level conditions. The tests described in this study were conducted on the horizontal rig to prevent an oscillating transition (flip-flop) which was observed in former dual bell tests performed in the high-altitude chamber.

Dry nitrogen was used as the working fluid, stored in high-hyphpressure vessels under ambient temperature conditions. The maximum feeding pressure was 5.5 MPa. The flow passes a settling chamber, a cross-section constriction, and a bending tube section before it accelerates in the convergent–divergent nozzle to supersonic velocity (Figs. 5 and 6). To study both operating modes, transition from the sea level mode to the high-altitude mode as well as the retransition back to sea level mode, the feeding pressure P_0 was regulated up and down with a constant gradient.

As P_a was constant during a test run, the variation of the nozzle pressure ratio (NPR, P_0/P_a) was directly proportional to the variation of P_0. The test facility features P_0 gradients up to ± 0.25 MPa/s. Figure 7 gives a typical test profile with a successively increased feeding pressure up to transition conditions and a subsequently decreasing shut down. The abrupt wall pressure variations in the extension (wall pressure signal P_{w9}) indicate transition: pressure drop due to the presence of the highly expanded flow at the wall and retransition: pressure rise due to the flow separation and the recirculation of ambient air at the extension wall. The pressure port P_{w9} is positioned in the middle of the dual bell extension and reacts on the moving flow separation front.

All three nozzle contours were tested under similar conditions to perform a parametric study. The nozzle models were tested for each configuration under various feeding pressure gradients: ± 0.2 MPa/s, then ± 0.1 MPa/s and ± 0.05 MPa/s, to study the influence of the pressure variation on the transition behavior.

B. Test Specimens

Various geometrical parameters have to be considered for the understanding of dual bell nozzle behavior. The use of the horizontal test rig at *P*6.2 limits the possibilities for some of these parameters: the throat radius should not exceed 10 mm (maximum mass flow limitation) and the transition must occur at a value of the pressure

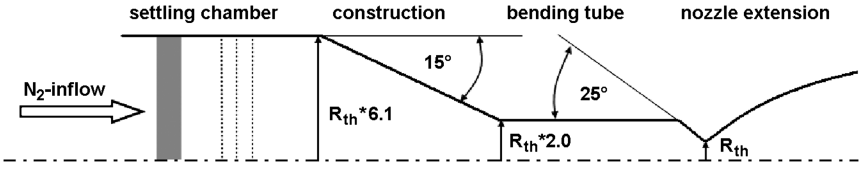

Fig. 5 Sketch of horizontal test rig.

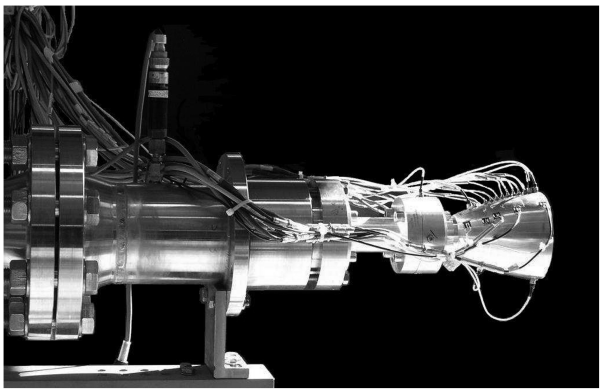

Fig. 6 Horizontal test rig at P6.2 test bench.

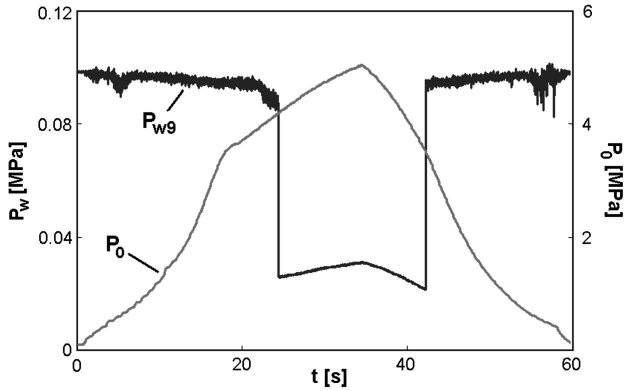

Fig. 7 Variation of feeding and wall pressure during a typical test run.

ratio P_0/P_a lower than 55 (installation maximum NPR). The remaining parameters are the base nozzle and extension length L_b and L_e, the inflection angle α, and the base and extension area ratios ϵ_b and ϵ_e (see Fig. 8).

Three dual bell nozzle models were tested for this study, referred to as contour DB1, DB2, and DB3 and presenting different geometrical parameters [9]. The common base nozzle was designed as a TIC (truncated ideal contour) nozzle using an inhouse code based on the method of the characteristics. The design inputs were the throat radius $R_{\text{th}} = 10$ mm and the design Mach number $M_d = 5.8$, for the total conditions $T_0 = 293$ K and $P_0 = 5$ MPa, under 1 bar ambient pressure.

A TIC base nozzle generates, contrary to a thrust optimized parabola (TOP) base nozzle, no internal shock system that would interfere with the oblique separation shock originated at the contour inflection during sea level mode.

The nozzle extension features a constant pressure (CP) wall profile. It was designed as a freejet isobar leaving the last point of the base nozzle contour. The isobar can be found by increasing the contour inflection angle inducing a Prandtl–Mayer expansion. As the resulting Mach number and wall pressure cross the chosen extension separation criterion, the isobar is reached. This procedure assures a flow transition at a given ambient pressure for a given nozzle total pressure, i.e., for a given NPR. The nozzle itself was made of acrylic glass with a wall thickness of 10 mm.

The geometric parameters investigated within this study are the base length L_b, the extension length L_e, and the inflection angle α.

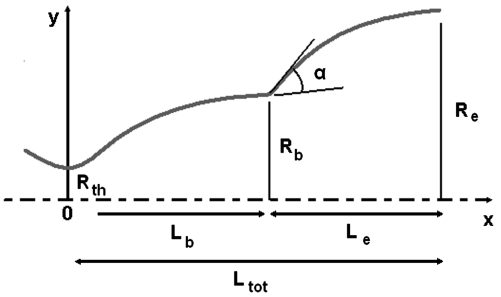

Fig. 8 Geometrical parameters of a dual bell nozzle.

The contour geometries were chosen with a common initial value of the extension length $L_e/R_{\text{th}} = 8.3$. The geometric parameters of the three tested nozzle contours (DB1, DB2, and DB3) are summarized in Table 1.

In addition, the contour extensions have been successively shortened (DB1 and DB2 in four, DB3 in six steps) and tested under the same conditions to investigate the influence of the extension length. Table 2 summarizes the relative extension lengths $L' = L_e/L_{\text{tot}}$ for each nozzle model.

The truncation has been shown in a former study [10] to have no fundamental influence on the flow behavior.

C. Instrumentation

The nozzle was equipped with pressure measurement ports along a streamline from the nozzle throat to its exit. To achieve better resolution in the vicinity of the contour inflection, further positions in the other quadrants were applied (0, 90, 180, and 270°). The measurement ports are labeled from $P_{w,b1}$ to $P_{w,b9}$ in the base nozzle (respectively, $P_{w,b1}$ to $P_{w,b7}$ for contour DB3) and from P_{w1} to P_{w12} in the extension. Piezoresitive "Kulite Semi-Conductor Inc." transducers (model XT-154-190M) were screwed into the nozzle wall. They were in contact with the fluid via 0.5 mm wall orifices. Positions $P_{w,b1}$ to $P_{w,b3}$ were recorded with transducers of an operational

Table 1 Contour geometry of the three tested nozzles in their design configuration

		DB1	DB2	DB3
Throat radius	R_{th}	10 mm	10 mm	10 mm
Area ratio	ϵ_b	11.3	11.3	9.4
	ϵ_e	27.1	24	25.6
Base length	L_b/R_{th}	6.2	6.2	5.2
Total nozzle length	$L_{\text{tot}}/R_{\text{th}}$	14.5	14.5	13.5
Inflection angle	α	7.2°	5°	7.2°

Table 2 Successive relative extension length L' of contours DB1, DB2, and DB3

Series	DB1	DB2	DB3
1	0.57	0.57	0.61
2	0.53	0.48	0.56
3	0.49	0.39	0.49
4	0.41	0.23	0.41
5			0.3
6			0.16

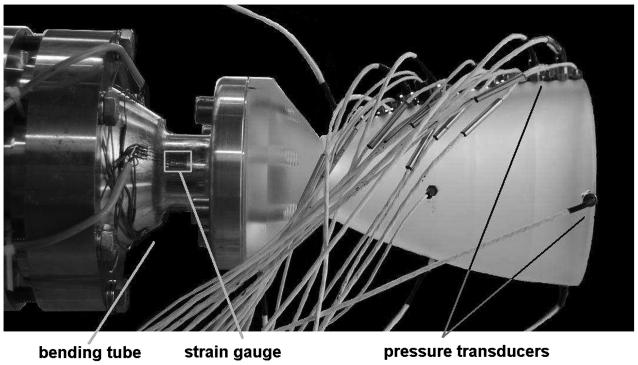

Fig. 9 Dual bell model with its instrumentation during mounting on the test bench.

pressure range up to 2 MPa. The remaining transducers have a range of 0.1 MPa. The transducer accuracy in this operating range is 0.5%. The signals were recorded with a rate of 1 kHz for low-frequency measurements and 25 kHz for high-frequency measurements. The signals were low-pass filtered at 160 and 8 kHz, respectively. The natural frequency of the transducers is 150 kHz.

To qualify the dual bell nozzle for rocket engine application, its side load generation during flow transition is the most critical feature. For this reason, side load measurements were a focus of this work. A thin-walled bending tube, sensitive to lateral forces, was placed upstream of the converging part of the nozzle (Fig. 9) enabling bending movements generated by flow instabilities and asymmetries. Details are illustrated in Fig. 10. The experience from previous tests led to an optimized measurement system. A rather short bending tube was used irrespective of the small moment generated, such that the signal was associated with low amplitude. Indeed, the short tube features a higher eigenfrequency (about 250 Hz). This is outside the measurement domain and can be low-pass filtered by the amplifiers (at 160 Hz).

Pairs of strain gauges were placed on opposite sides of the tube wall (in the vertical as well as the horizontal direction) and connected into a full Wheatstone bridge. The measurement signal was directly proportional to the bending deformation. Other components, such as tension, compression, torsion, or temperature impact were compensated by the circuit arrangement. The resolution obtained with this setup is 0.2 N, with a deviation of 0.3 N.

The generated force and its natural oscillation frequency can be related to the recorded electrical signal with an appropriate transfer function (see details in Frey et al. [11]). However, the side load measurements strongly depend on the setup and the nozzle model (wall thickness, mass, material) and cannot be directly scaled to a real rocket engine configuration. This can be circumvented by relating the measured side loads to an equivalent force acting at the nozzle exit.

The side load measurement setup was calibrated by bending the nozzle with three weight forces applied at the nozzle end. The connecting string was cut during signal recording, giving dynamic and static behavior. The results presented in this work are given in Newtons and correspond to the reference force at the nozzle end in its initial configuration (before truncation).

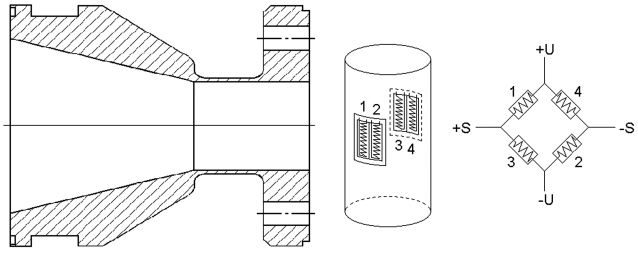

Fig. 10 Detail of the bending tube.

In addition, a schlieren optic installation was used to observe, in detail, the flow evolution during the transition from one mode to the other. The shock system downstream of the truncated nozzle extension was recorded during mode transition via black and white schlieren optics. A high-speed camera with a maximum recording frequency of 2000 frames/s was triggered at the onset of transition by a pressure sensor chosen in the extension.

III. Results and Discussion

A. Side Loads Phenomenology

1. *Operating Modes*

For each test, the NPR was progressively increased and decreased to study the evolution of the flow along the nozzle wall (see pressure distribution in Fig. 11 for nozzle model DB3). During startup of the nozzle the flow attaches progressively to the base wall and the flow separation moves downstream. As the separation front reaches the contour inflection its movement is initially stopped, despite a further increase of the nozzle feeding pressure. The flow is completely attached to the base nozzle wall and separated within the extension: sea level mode is reached. Exemplary normalized wall pressure measurements are given in Fig. 11. The base nozzle wall pressure (for $x/R_{\text{th}} < 5.2$) corresponds to the classical distribution in conventional nozzles. Within the extension, the recirculating flow is characterized by a more or less constant pressure at the nozzle wall, slightly lower than the ambient pressure P_a.

When further increasing the NPR, the flow pattern suddenly changes to high-altitude mode. The very low extension wall pressures indicate the presence of the overexpanded flow. The pressure decrease in the extension is very fast, dropping instantly upon transition (see Fig. 7).

By decreasing the nozzle feeding pressure P_0, flow retransition occurs. The flow separation front rapidly moves back to the contour inflection. The operating mode changes back to sea level mode.

Figure 12 gives a typical test profile with up and downramping of NPR (here for contour DB2 with a gradient of ± 0.2 MPa/s). The nozzle startup and shut down generates for NPR values between 2.5 to 7 relatively high side loads. The averaged value is 10 N and peak values reach 40 N. Such high loads are due to the transition of the boundary layer in the throat region from laminar to turbulent, which leads to a partial flow reattachment, as described by Stark and Wagner [10]. By increasing the NPR (from 8 to about 30), the flow progressively attaches to the base nozzle wall. The sea level mode is reached for a NPR value of 30. The flow is fully attached in the whole base nozzle and separates in a controlled manner at the inflection. The side load amplitude is low, about 4 N.

The transition occurs at $\text{NPR}_{\text{tr}} = 41.3$ and generates a very high side load peak, over 100 N, corresponding to over three times the side load amplitude for small NPR values. The transition duration is very short, typically in the order of some milliseconds. Once the high-altitude mode is reached, the flow is attached all the way to the nozzle end and the side loads are very low, with an amplitude of about 2 N.

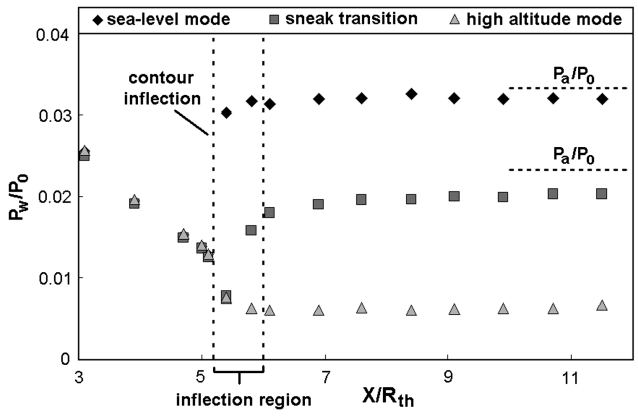

Fig. 11 Wall pressure distribution for various NPR values.

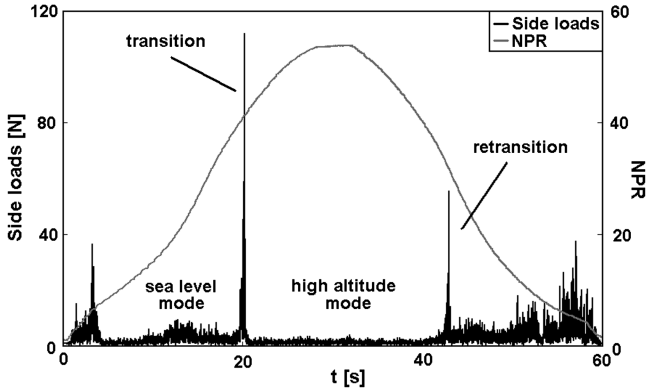

Fig. 12 Side load generation during a typical test run (NPR up and down ramping).

The retransition occurs for a NPR value lower than the transition, here $\mathrm{NPR}_{\mathrm{retr}} = 31.7$, and leads back to sea level mode.

2. Transition and Retransition

The transition NPR can be calculated with Eq. (1), using a separation criterion for conventional nozzles, e.g., Stark and Wagner [10] ($P_{e,\mathrm{sep}}/P_a = 1/M_e$), where the flow separation is a function of the related wall Mach number (here the extension wall Mach number M_e)

$$\mathrm{NPR}_{\mathrm{tr}} = P_0/P_{a,\mathrm{tr}} = \frac{P_0}{P_e}\frac{P_{e,\mathrm{sep}}}{P_a} = \frac{P_0}{P_e}\frac{1}{M_e} = \frac{1}{M_e}\left(1 + \frac{\gamma - 1}{2}M_e^2\right)^{\frac{\gamma}{\gamma-1}} \tag{1}$$

The constant wall pressure within the extension nozzle leads to a fast transition from one operating mode to the other. The separation conditions are the same for every point in the nozzle extension: as the conditions are exceeded at one point of the extension, they are exceeded at every point. The asymmetrical and fast movement of the separation front during transition from sea level to high-altitude mode is responsible for the significant side load peak.

The performed high-speed schlieren measurements yield information of the separation front evolution within the nozzle extension during transition. Figure 13 is an image taken during flow transition. The image was overlaid with a nozzle contour grid; the shock was marked and elongated to the extension wall (left). The location of the separation point shows a significant asymmetry, with an order of magnitude of $\Delta x/R_{\mathrm{th}} \approx 1$. The asymmetry of the separation leads to a small asymmetry of the Mach disk resulting in a jet deflection.

The retransition occurs for a much lower NPR, leading to a hysteresis effect related to the transition NPR. The hysteresis effect is one of the dual bell's major features as it assures a stable transition to high-altitude mode being able to withstand a certain level of NPR variations induced by either combustion chamber or ambient pressure fluctuations (e.g., during buffeting). However, the process of retransition is up to now not well understood and not predictable. The side load peak of retransition is in most cases lower than the transition peak and only of interest for ground testing and not for real flight application.

3. Sneak Transition

Tests conducted with a low NPR gradient exposed a third flow condition between sea level and high-altitude mode. Figure 14 illustrates the theoretical and measured wall pressure distribution in the vicinity of the contour inflection in a full flowing dual bell nozzle. Because of viscosity effects within the boundary layer, the wall pressure trend has a finite negative gradient and not a discontinuity like theoretically expected. This effect was already predicted by Martelli et al. [8] within a numerical study. In sea level mode, the separation front is stabilized at the contour inflection for a wide range of NPR. When further increasing the NPR, the separation front starts moving downstream of the contour inflection, and the wall pressure drops in this region (Fig. 11). A further increase of the NPR leads to the actual transition and the abrupt flow attachment to the whole nozzle extension. So, for a certain interval of NPR, the separation can find a stable position in the so-called inflection region [7] (Fig. 14). This flow evolution preceding the actual transition is addressed as sneak transition [9]. The dual bell nozzle extension must be divided into two parts: the inflection region, where the wall pressure gradient is negative, and the residual part of the extension, where the wall pressure is constant.

In real rocket engine applications, the total pressure stays constant during ascent. The variation of NPR is only due to the variation of the ambient pressure with altitude change. This variation is very slow, such that the sneak transition will be another critical issue for the qualification of the dual bell nozzle concept.

The sneak transition can be the source of high side loads of the same magnitude as those encountered during startup. Figure 15 represents the evolution of the wall pressure in the inflection region (namely first sensor downstream of the inflection, P_{w1}), in the constant pressure region of the extension (sensor position P_{w11}) and the related side loads in nozzle DB2. Before $t = 26.5$ s, the nozzle operates in sea level mode and the side loads are smaller than 5 N. The sneak transition starts as the P_{w1} pressure drops. The separation front has left the contour inflection and is no longer symmetrical. The side load amplitude increases with peaks over 30 N. The side load peak of the actual transition corresponds to the pressure drop of P_{w11}. After

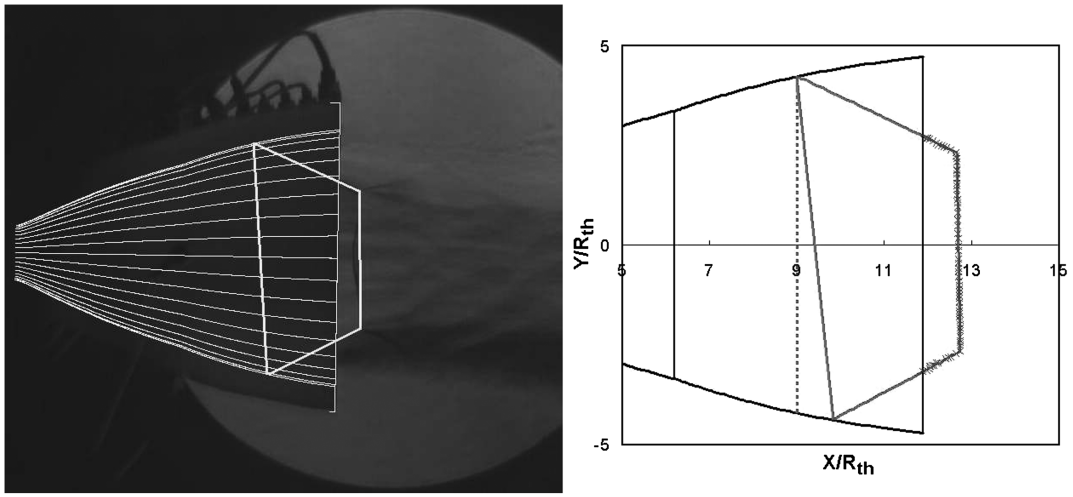

Fig. 13 Schlieren observation of the shock system within a truncated nozzle during flow transition.

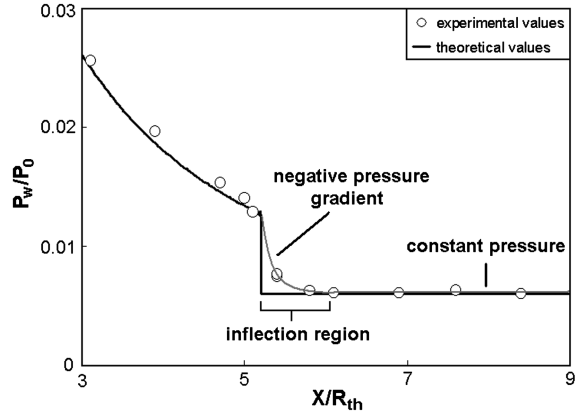

Fig. 14 Negative wall pressure gradient in the inflection region.

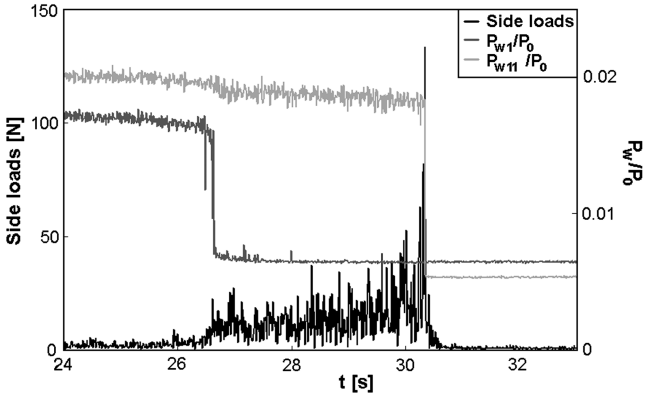

Fig. 15 Side load and wall pressure measurements during sneak transition.

transition has occurred, the side loads are once again significantly reduced.

Side load measurements have been made with the same installations on a truncated ideal nozzle by Stark and Wagner [10]. The geometrical parameters are presented in Table 3 together with the parameters of the dual bell. The nozzle geometries are close and the side loads generated from these nozzles are comparable.

Figure 16 compares the side loads measured for the TIC and the dual bell nozzle, as a function of NPR. The startup side loads present similar amplitudes: 30–40 N for NPR values up to 7. While increasing the NPR, the separation front moves downstream. The TIC is fully attached for a NPR of about 50 and the dual bell base nozzle for a NPR of 30. The side loads generated in the TIC during the separated flow regime are 3 times higher compared with the dual bell. However, the dual bell transition to high-altitude mode leads to a side load peak that is twice as high as the maximum side load of the TIC. The sneak transition leads to side loads of the same magnitude as a separated TIC (see detail). Once the high-altitude mode is reached, the side loads in the dual bell are much lower than those of a full flowing TIC.

The operation of a dual bell nozzle can be divided into five phases: the two operating modes, sea level and high-altitude mode, the sneak transition, the actual transition, and the retransition. Both operating modes are characterized by very low side load amplitude, transition

Table 3 Nozzle geometry comparison

		TIC	DB2
Throat radius	R_{th}	10 mm	10 mm
Area ratio	ϵ_e	20	24
Total length	L_{tot}/R_{th}	14.24	14.5

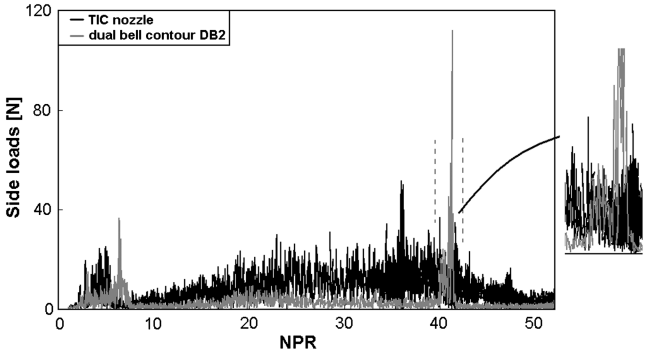

Fig. 16 Comparison of the side load generation between dual bell and TIC nozzles.

and retransition by a high-amplitude side load peak and sneak transition by side loads similar to conventional separated nozzles.

B. Design Parameters

The influence of the geometric parameters for side load generation is illustrated in Fig. 17 for representative measurements of each nozzle model (for a feed pressure gradient of 0.2 MPa/s). The side load measurements are presented as a function of the NPR during up-ramping ($dP_0/dt > 0$) for the three nozzle contours in their initial configuration ($L_e/R_{th} = 8.3$). Contours DB1 and DB2 possess the same base nozzle length $L_{b1}/R_{th} = L_{b2}/R_{th} = 6.2$ and different inflection angles ($\alpha_1 = 7.2°$ and $\alpha_2 = 5°$). Contours DB1 and DB3 present the same inflection angle, but a different base geometry ($L_{b3}/R_{th} = 5.2$).

At low NPR values (between 2.5 and 7), the nozzles generate moderate side loads: for all three nozzle contours the averaged value is 10 N and peak values reach 40 N. The tested nozzles all presented the same geometry in the throat region and hence comparable side loads at low NPR values. By increasing the NPR, the separation point progressively moves down along the base nozzle wall. For NPR values between 8 and 30, the flow progressively attaches in the base nozzle generating side loads with low amplitude. Sea level mode is characterized by very low side load amplitude. The high side load peak indicates the transition at NPR values between 40 and 50, depending on the contour geometry [12]. Before the transition peak, the sneak transition takes place, characterized by higher side loads, around 30 N for every configuration. The amplitude of the side loads during sneak transition seems to be independent of the nozzle geometry.

The right side of Fig. 17 is a magnification of the sea level mode. The measurements for contours DB1 and DB3 are comparable. The values of the side loads are significantly higher for contour DB2. The higher inflection angle α of contours DB1 and DB3 lead to larger recirculation area and thus a lower side load amplitude under sea level mode. Decreasing the value of α increases the amplitude of the side loads during sea level mode.

Figure 18 depicts the side load generation for decreasing NPR values ($dP_0/dt < 0$). The side load amplitude is very low during high-altitude mode, for NPR values higher than 40 for contour DB1, respectively, 30 for contours DB2 and DB3. The magnified area shows that no amplitude difference appears for the various geometries. As long as the flow is attached to the extension wall, the geometrical parameters L_b and α have no influence on the side load generation for the three nozzle models.

The low NPR side loads (NPR < 7) are comparable in amplitude with those measured when increasing the NPR and show no dependency on the dual bell nozzle geometry.

For all three nozzles tested in this study, the strain gauges have been calibrated for the nozzle at its initial full length. The values presented correspond to the equivalent static force acting at the nozzle end, perpendicular to the symmetry axis. The shortened configurations are related to the full length configuration for easier comparison of the measured forces.

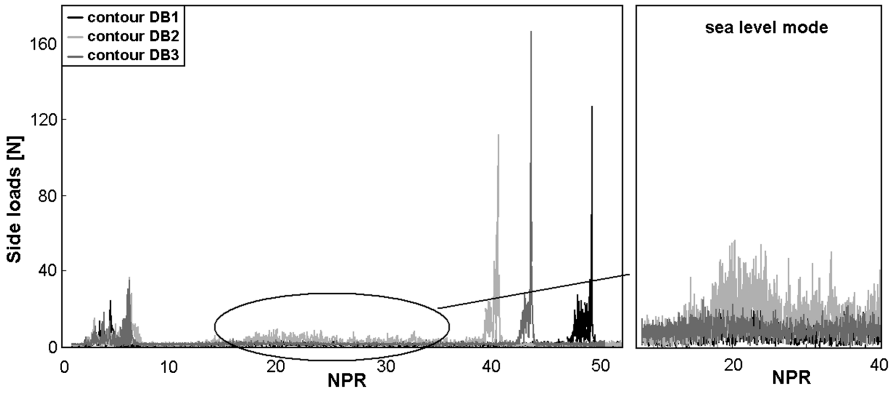

Fig. 17 Side load measurements during up-ramping for various dual bell nozzle geometries.

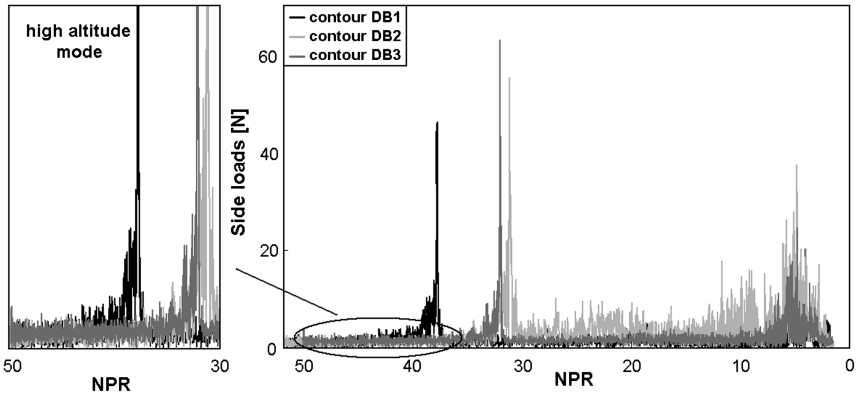

Fig. 18 Side load measurements during downramping for various dual bell nozzle geometries.

The side loads generated by nozzle DB2 under its various length configurations (from $L' = 0.57$ down to $L' = 0.23$) are presented in Fig. 19. The measurements are given as a function of the NPR, for a positive gradient ($dP_0/dt > 0$) on the left and a negative one ($dP_0/dt < 0$) on the right.

At low NPR and during sea level mode, the side loads generated are lower for the shorter nozzle configurations, due to the smaller lever arm. The transition occurs for lower NPR values in the initial length as shown in a former study by the authors [9]. The peak amplitude decreases when decreasing the extension length. In the shorter configuration ($L' = 0.23$), as no actual transition takes place, no peak in the side loads was measured. In high-altitude mode, the side loads are very low and comparable for all configurations.

The second graphic in Fig. 19 (right) depicts a similar side load evolution for decreasing NPR values. The high-altitude mode still generates very low side loads. Retransition is reached for the shorter configurations first ($\mathrm{NPR_{retr}} = 46$ for $L' = 0.23$ and 40 for $L' = 0.39$). A side load peak marks the flow retransition to sea level mode. However, its amplitude seems to be lower than the transition peak. Sea level mode is characterized by moderate side loads. For the longest configuration, the NPR values of retransition and separation at the base nozzle end are close ($\mathrm{NPR_{retr}} = 32.5$ and NPR separation at the base nozzle end is about 30), so the sea level mode is difficult to discern. The flow separation moves upstream to the throat when the NPR value is further decreased. At low NPR values (between 7 and 2.5), the nozzle generates higher side loads with peak amplitude of up to 40 N in the longest configuration and up to 20 N in the shorter ones.

The asymmetrical displacement of the separation point in the extension during the transition is the cause of the side load peak. The increase of the extension length leads to a longer region of potential asymmetry. The generation of side loads depends on the dual bell geometry: the longer the extension, the higher the peak in the side loads during both transition and retransition.

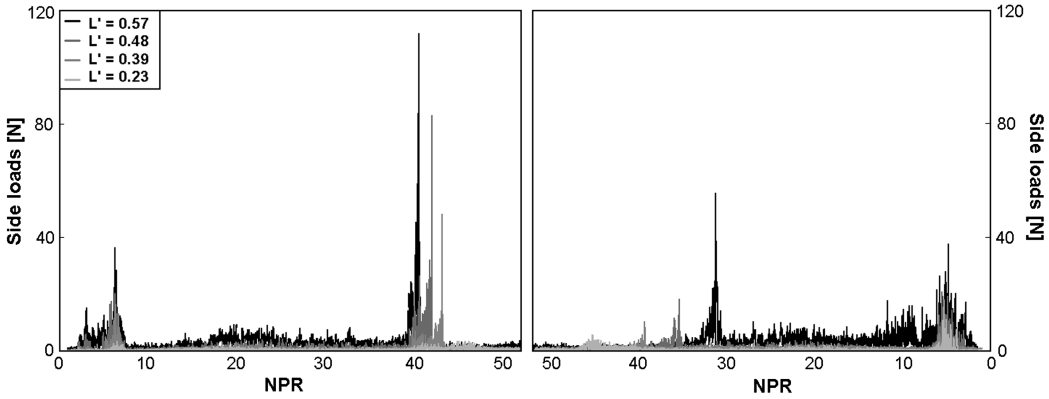

Fig. 19 Side load measurements for various nozzle lengths for increasing (left) and decreasing (right) NPR.

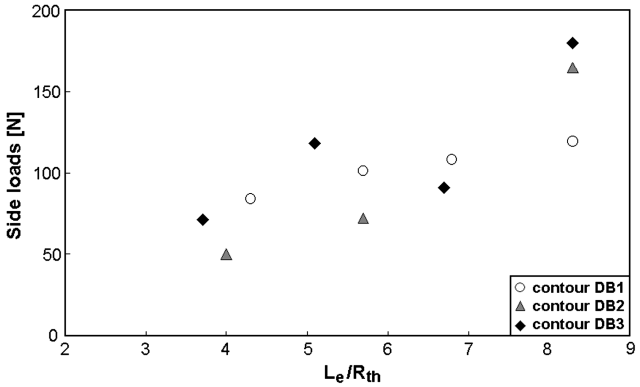

Fig. 20 Amplitude of the transition side load peak for various nozzle configurations.

For each nozzle configuration, the amplitude of the transition peak has been measured. Figure 20 depicts the average value of the peak in side loads as a function of the extension length.

An increase in the peak amplitude can be seen for all three nozzles. However, the transition from one mode to the other is very fast and it is difficult to estimate the precise peak amplitude with the measurement system. In particular, the test series with nozzle contour DB3 shows the most variations in the trend, with measurement divergence up to 30% from the mean values. This effect is due to the lowest acquisition rate (1 kHz) used for this first test series. The measurements on contours DB1 and DB2 were then recorded with a higher value of acquisition rate: 25 kHz, which leads to smaller variations (up to 15%).

Figure 21 depicts the peak amplitude in nozzle contour DB2 for a representative configuration (here $L' = 0.39$) as a function of the NPR gradient. The gradient does not seem to have any significant influence on the amplitude of the peak in side loads during the transition.

The transition from one operating mode to the other is the critical phase in the dual bell nozzle operation. The peak in side loads has to be limited in amplitude and duration to avoid damage to the engine and payload. Therefore, the extension length is the determining parameter for side load peak reduction.

C. Transition Duration and Stability

Beside side load generation, the transition duration and the stability of the two modes toward NPR fluctuation (hysteresis between $\mathrm{NPR_{tr}}$ and $\mathrm{NPR_{retr}}$) must be precisely known for dual bell qualification.

The transition and retransition are defined as the instant when the pressure jumps abruptly at the measurement positions along the extension wall. The relative gap between the transition and retransition NPR is crucial for the stability of the flow mode. A significant hysteresis should avoid a variation of the NPR, due for example to P_0 variation caused by combustion fluctuations or to P_a variation due to buffeting effect around the rocket during flight, leading to an oscillation from one operating mode to the other. To evaluate the stability of a dual bell flow, the value of the hysteresis is calculated as the ratio of the difference between transition and retransition NPR over $\mathrm{NPR_{tr}}$

$$\text{hysteresis} = \frac{\mathrm{NPR_{tr}} - \mathrm{NPR_{retr}}}{\mathrm{NPR_{tr}}} 100 \tag{2}$$

The values of the transition and retransition NPR were recorded for each nozzle configuration and the hysteresis percentage was then calculated. The measured hysteresis values are displayed in Fig. 22 for every nozzle configuration as a function of the relative extension length $L' = L_e/L_{\mathrm{tot}}$. The given values are averaged for each configuration with a maximum experimental error of less than 2.5%. The hysteresis value increases with L', for every nozzle configuration tested.

The extension length L_e, and more precisely the relative length L', is the outstanding parameter for the improvement of dual bell nozzle flow stability. The gap between transition and retransition NPR can be increased by increasing the length of the dual bell extension.

The estimation of the transition duration is also critical for the prediction of the structural life time. As seen in the previous section, the flow can present, during the transition from one mode to the other, significant asymmetries that lead to high side loads. To prevent damage to the nozzle structure, the transition duration should be minimized.

The high-frequency wall pressure measurements along the extension allowed the observation of the flow separation point displacement in the extension and the calculation of the time needed for the flow to achieve complete flow transition. Two duration values can be defined: the actual transition duration t_{tr} and the total transition duration t_{tot}.

The total transition duration t_{tot} corresponds to the time between the instant when the flow separation point first moves into the extension and the instant when it reaches the nozzle end (duration of transition including duration of sneak transition). The start of the transition is approximated with the pressure drop at the first sensor position in the extension. It corresponds to the time during which the separation point is located in the extension, potentially generating high side loads. The actual transition duration t_{tr} is measured between the instant when the flow separation point leaves the inflection region and the instant when it reaches the nozzle extension end. In this interval, the separation point is located in the constant pressure region of the extension. The maximum separation point asymmetry at the nozzle wall may reach the whole extension length and leads to high side load peak. The actual transition duration is very short, in the range of milliseconds and increases with decreasing extension length.

The averaged total transition duration has been calculated for every configuration. The total transition duration decreases linearly with increasing extension length, which is the opposite of the

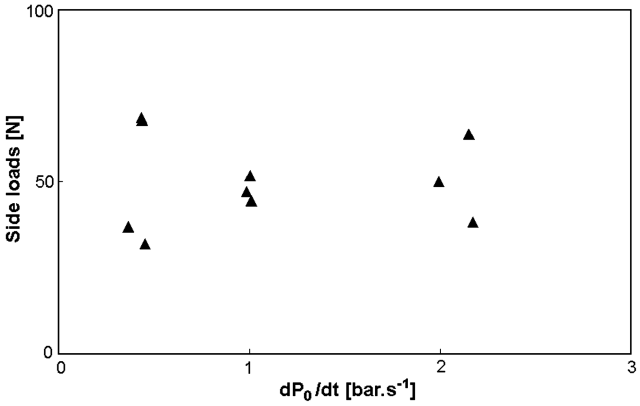

Fig. 21 Side load peak as a function of the NPR gradient for dual bell model DB2.

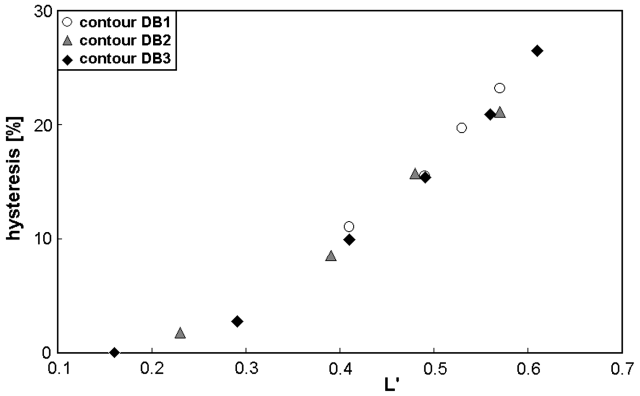

Fig. 22 Hysteresis between transition and retransition NPR as a function of the relative extension length.

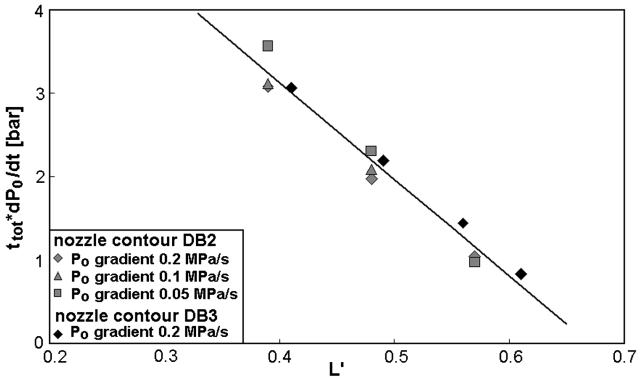

Fig. 23 Transition duration as a function of the NPR gradient and the relative extension length.

expected effect. The nozzle models were tested with feed pressure gradients: +0.2 MPa/s, +0.1 MPa/s, and +0.05 MPa/s. The total duration increases with decreasing gradient. The product of the total duration and the feed pressure gradient is plotted over the relative extension length for nozzle contour DB2 and DB3 in Fig. 23. The value of this product varies linearly with L' for the two nozzle geometries. The transition duration appears to be only a function of the extension length and the variation gradient of the NPR.

For the same pressure gradient, nozzles DB2 and DB3 show a similar behavior. The base nozzle length L_b and the inflection angle α have no significant influence on the total transition duration.

Two of the most important parameters for the optimization of the dual bell concept show a good correlation: transition stability and duration can be improved by increasing the length of the extension nozzle. However, the variation gradient of the NPR has to be high enough to reduce the transition duration.

D. Critical Influence of Extension Length

The base nozzle geometry (throat radius R_{th}, design Mach number M_d, and base length L_b) defines the performance of a dual bell during sea level mode. The inflection angle α determines the transition conditions and the performance during high-altitude mode. The other transition phenomena are dominated by the length of the dual bell nozzle extension L_e, also expressed as the relative extension length L'.

Figure 24 illustrates the evolution of the transition duration and the side load peak amplitude with the relative extension length L' for nozzle contour DB1. This graphic points out the necessity of a tradeoff between side load peak duration and amplitude.

Increasing the relative extension length leads to a high transition side load peak, during a very short time. The amplitude of the peak can be decreased by increasing L' but the duration of the loads will also be increased.

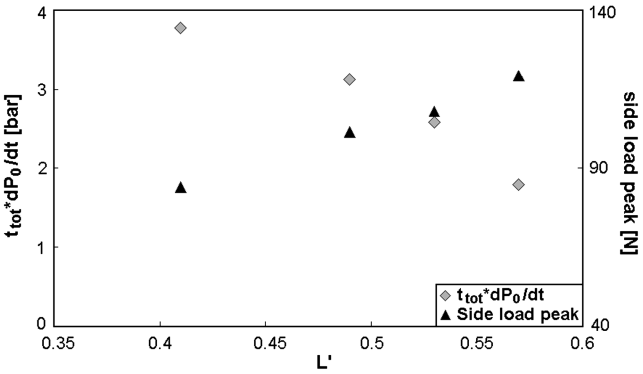

Fig. 24 Comparison of the transition duration and the side load peak amplitude for nozzle DB1.

IV. Conclusions

The dual bell nozzle concept was found to be one of the most promising candidates to achieve an impulse gain for main stage rocket engines at sea level as well as high-altitude mode. Its contour inflection enables a one-step altitude adaption without any moving parts and minor impact on the design of already operational rocket engines. One of its main features is a hysteresis between transition and retransition NPR, which stabilizes the transition and allows the dual bell to withstand a certain level of pressure fluctuations, e.g., due to buffeting. The transition NPR is predictable, but the process of retransition is up to now not well understood and has to be studied more in-depth in future.

This cold flow experimental study has shown the different phases of operation of dual bell nozzles and the side load generation corresponding to each phase. In its operating modes, a dual bell nozzle produces smaller side loads than a conventional TIC nozzle. However, the transition goes ahead with a short time side load peak that must be taken into account to avoid harm to the engine structure.

A third mode was experimentally confirmed, addressed as sneak transition. Sneak transition is an intermediate state preceding the actual transition to high-altitude mode, with side loads comparable to separated conventional nozzles. As the NPR gradient in real flight application is very low, the sneak transition becomes a critical issue. One possibility to reduce its duration, or even to avoid it, is to suddenly increase the NPR and therefore to force an immediate transition. For this reason, throttleable rocket engines are in favor.

The side load amplitude in sea level mode can be reduced by choosing a higher value of the inflection angle. The extension length was found to be the outstanding parameter for contour optimization. The stability of the two operating modes and the duration of the transition can be enhanced by increasing the extension length. However, this increase leads also to higher amplitude peaks in side loads during transition and retransition. A tradeoff will have to be found between stability of the modes, the amplitude of the peak in side load and the duration of the transition.

Acknowledgment

Financial support has been provided by the German Research Foundation (Deutsche Forschungsgemeinschaft: DFG) in the framework of the Special Research Field Transregio 40.

References

[1] Foster, C., and Cowles, F., "Experimental Study of Gas-Flow Separation in Overexpanded Exhaust Nozzles for Rocket Motors," Jet Propulsion Laboratory, Progress Rept. 4-103, 1949.

[2] Horn, M., and Fisher, S., "Dual-Bell Altitude Compensating Nozzles," Rocketdyne Division, NASA CR-194719, 1994.

[3] Frey, M., and Hagemann, G., "A Critical Assessment of Dual-Bell Nozzles," *Journal of Propulsion and Power*, Vol. 15, No. 1, pp. 137–143.
doi:10.2514/2.5402, 1999.

[4] Hagemann, G., Terhardt, M., Haeseler, D., and Frey, M., "Experimental and Analytical Design Verification of the Dual-Bell Concept," *36th AIAA Joint Propulsion Conference*, AIAA Paper 2000-3778, July 2000.

[5] Hieu Le, T., Girard, S., and Alziary de Roquefort, T., "Direct Measurement of Side Loads with Transonic Buffeting," *5th European Symposium on Aerothermodynamics for Space Vehicles*, European Space Agency, Noordwijk, The Netherlands, Nov. 2005.

[6] Karl, S., and Hannemann, K., "Numerical Investigation of Transient Flow Phenomena in Dual-Bell Nozzles," *6th International Symposium on Launcher Technologies*, European Space Agency, Noordwijk, The Netherlands, 2005.

[7] Martelli, E., Nasuti, F., and Onofri, M., "Numerical Parametric Analysis of Dual-Bell Nozzle Flows," *AIAA Journal*, Vol. 45, No. 3, pp. 640–650.
doi:10.2514/1.26690, March 2007.

[8] Martelli, E., Nasuti, F., and Onofri, M., "Numerical Analysis of Film Cooling in Advanced Rocket Nozzles," *AIAA Journal*, Vol. 47, No. 11, pp. 2558–2566.
doi:10.2514/1.39217, 2009.

[9] Nürnberger-Génin, C., and Stark, R., "Experimental Study on Flow Transition in Dual Bell Nozzles," *Journal of Propulsion and Power*,

Vol. 26, No. 3, pp. 497–502.
doi:10.2514/1.47282, May–June 2010.
[10] Stark, R., and Wagner, B., "Experimental Study of Boundary Layer Separation in Truncated Ideal Contour Nozzles," *Shock Waves*, Vol. 19, No. 3, pp. 185–191.
doi:10.1007/s00193-008-0174-6, 2008.
[11] Frey, M., Stark, R., Cieski, H., Quessard, F., and Kwan, W., "Subscale Nozzle Testing at the P6.2 Test Stand," *36th AIAA Joint Propulsion Conference*, AIAA Paper 2000-3777, July 2000.
[12] Nürnberger–Génin, C., and Stark, R., "Flow Transition in Dual Bell Nozzles," *Shock Waves*, Vol. 19, No. 3, pp. 265–270.
doi:10.1007/s00193-008-0176-4, 2008.

J. Powers
Associate Editor